Adaptive observations in the context of 4D-Var data assimilation

Dacian N. Daescu

Institute for Mathematics and its Applications
University of Minnesota
Minneapolis, MN 55455, USA

I. M. Navon*

Dept. of Mathematics and School of Computational Science
and Information Technology , Florida State University
Tallahassee, FL 32306, USA

August 1, 2002

With 14 figures

*Corresponding author: School of Computational Science and Information Technology, Florida State University, Tallahassee, FL 32306-4120

Abstract

The design of adaptive observations strategies must account for the particular properties of the data assimilation method. A new adjoint sensitivity approach to the targeted observations problem is proposed in the context of four-dimensional variational data assimilation (4D-Var). The method is based on a periodic update of the adjoint sensitivity field that takes into account the interaction between time distributed adaptive and routine observations. Information provided by all previously located observations is used to identify best locations for new targeted observations. Adaptive observations at distinct instants in time are selected in a sequential manner such that the method is only suboptimal. The selection algorithm proceeds backward in time and requires only one additional adjoint model integration in the assimilation window. Therefore, the method is very efficient and is suitable for practical applications. A comparative performance analysis is presented using the traditional adjoint sensitivity method as well as the total energy singular vectors technique as alternative adaptive strategies. Numerical experiments are performed in the twin experiments framework using a two-dimensional global shallow water model in spherical coordinates and an explicit Turkel-Zwas discretization scheme. Data from a NASA 500mb analysis valid for 00Z 16 Mar 2001 6h obtained with the GEOS-3 model was used to specify the geopotential height at the initial time and the initial velocities were obtained from a geostrophic balance. Numerical results show that the new adaptive observations approach outperforms traditional targeting methods in terms of forecast error reduction at the verification time and its implementation is feasible for large scale atmospheric models.

1 Introduction

Short term prediction of rapidly evolving meteorological events may be greatly improved by reducing the analysis errors in dynamically sensitive geographical regions. Adaptive (targeted) observations strategies aim to improve the forecast of numerical weather prediction (NWP) models by identifying optimal locations where additional observations resources must be allocated. The significant research dedicated recently to the adaptive observations problem is primary motivated by the fact that forecast failure of severe weather events (e.g. hurricane) may have dramatic economical and societal impacts. At the same time, the expansion of the current observational network and the design of future observing networks require an assessment of the value added by observational data to improve the models forecast. Expensive field-deployed resources can be utilized more effectively and the science success can be maximized by selecting an optimal observational network.

Mathematical framework and a rigorous statistical formulation of the adaptive observation problem is described by Berliner et al. (1999). However, implementation of optimal statistical methods may not be feasible in practice due to the difficulty to provide accurate estimates of the model and observational errors statistics, the large dimension of the state space used in NWP ($\sim 10^7$), and limited computational resources. Recent field experiments such as FASTEX (Joly et al. 1999), NORPEX (Langland et al. 1999) and WSRP (Szunyogh et al. 2001) provided real life applications where several feasible methods for adaptive observations were tested.

The main differences between the proposed targeting strategies consist in the sensitivity analysis technique used to identify the areas where the errors in the initial conditions are rapidly growing and will mostly influence the forecast over the verification domain.

Adjoint modeling has been proved to be an essential tool for developing adaptive observations strategies. The adjoint of the tangent linear model associated with the nonlinear forecast model was used to implement targeting methods using the dominant singular

vectors (Palmer et al. 1998, Buizza and Montani 1999), gradient (adjoint sensitivity) fields (Langland et al. 1999, Langland and Rohaly 1996) and sensitivity to observations (Baker and Daley 2000, Doerenbecher and Bergot 2001). Pu and Kalnay (2000) use the adjoint modeling and a quasi-inverse linear model approach (Kalnay et al. 2000) for targeting observations. A comparative analysis between targeted observations using the total energy singular vectors (TESV) and Hessian singular vectors (HSV) is presented in the recent work of Leutbecher et al. (2002).

The Ensemble Transform (ET) (Bishop and Toth 1999) and the Ensemble Transform Kalman Filter (ET KF) (Bishop et al. 2001) are adaptive techniques based on nonlinear ensemble forecasts. A comparison between the TESV and ET KF targeting methods is presented by Majumdar et al. (2002).

Despite recent advances in the theoretical formulation and implementation of targeting methods, the problem of the optimal adaptive sampling is a young discipline and many open questions remain to be addressed. Studies performed during the field experiments revealed the potential benefits that may be achieved using adaptive observations as well as various practical issues and shortcomings of the current targeting methodologies. The adaptive methods may be effective as long as the linearization of the nonlinear dynamical model along a control trajectory remains valid. Since in practical applications the verification time is selected at a 24h to 72h range, it is essential to establish the validity of the linear approximation before these methods can be efficiently used (Hansen and Smith 2000). The design of adaptive strategies must account for various factors such as: the forecast model details, the magnitude of the uncertainty in the initial conditions (Lorenz and Emanuel 1998), the uncertainty growth (Rabier et al. 1996), the data assimilation scheme used to provide the initial conditions (Bergot 2001), the configuration of the existing observational network (Morss et al. 2001), and the number of the additional observational resources to be allocated.

The characteristics of the data assimilation system may be integrated in the adap-

tive observations method by using the sensitivity to observations technique proposed by Baker and Daley (2000). This approach was studied for 3D-Var data assimilation by Doerenbecher and Bergot (2001) who emphasized that to optimize the efficiency of adaptive techniques the assimilation of both conventional and adaptive observations must be considered.

In this paper we investigate the design of an adaptive observations system given the configuration of the conventional observational network and assuming that four dimensional variational data assimilation (4D-Var) is performed. The TESV and ET KF targeting methods were considered in the 4D-Var context by Leutbecher et al. (2002) using a perfect model scenario and assuming that adaptive observations are available only in the middle of the assimilation period. Our work represents a first attempt to fully account for the temporal dimension of the 4D-Var scheme by considering time distributed adaptive observations. In particular, we show that the interaction between routine (fixed location) and targeted observations taken at distinct instants in time plays a significant role in the efficiency of the adaptive strategy. We design a simple mechanism to account for the interdependence between space and time distributed observations and further use it to implement an adjoint based targeting method. A comparative study with the traditional adjoint sensitivity (AS) and TESV methods is performed using a shallow water model. Our preliminary results indicate that at a reduced additional computational cost, the benefits of the new proposed targeting method on forecast error reduction may be significant.

The paper is organized as follows: in Section 2 we formulate the adaptive observations problem in the 4D-Var data assimilation context. The two-dimensional shallow-water model used in the numerical experiments is presented in Section 3. A perfect model scenario (twin experiments) is used to implement the data assimilation procedure and observations are provided using model generated data. In Section 4 we briefly review the AS and TESV methods for targeting observations. The interaction mechanism between time

distributed adaptive observations and fixed location observations is described in Section 5. A new adjoint-based targeting method using interactive adjoint sensitivity (IAS) fields is presented. In Section 6 we perform a comparative performance analysis between IAS, AS, and TESV targeting methods in two different scenarios: first, we assume that the adaptive observations are the only available observations to the data assimilation system; second, fixed location observations distributed on a sparse uniform subgrid are also included into analysis. Concluding remarks and further research directions are presented in Section 7.

2 4D-Var data assimilation and adaptive observations

Bergot (2001) studied the efficiency of adaptive observations using incremental 3D-Var and incremental 4D-Var data assimilation schemes (Courtier et al. 1994). The results obtained for a SV targeting method demonstrate that the sampling of the sensitive area and the assimilation scheme are intimately dependent. In this section we formulate the adaptive observations problem in the 4D-Var data assimilation context. We assume that a model forecast $\mathbf{x}^f = \mathcal{M}(\mathbf{x}^b)$ initiated at time t_0 from a background estimate $\mathbf{x}^b$ of the true atmospheric state $\mathbf{x}_0^t$ predicts a severe weather event at a future verification time $t_v > t_0$ over the verification domain $\mathcal{D}_v$.

In the analysis time interval $[t_0, T], T < t_v$ the conventional observing network provides a set of time distributed observations $\mathcal{O}^f$. We will refer to $\mathcal{O}^f$ as routine (fixed location) observations and the location of $\mathcal{O}^f$ is a priori known at the initial time t_0. In practical applications the length of the assimilation window $[t_0, T]$ is usually 6h, whereas the verification time t_v is selected at 24h to 72h range from t_0. We assume that at each time instant $t_i,\ t_0 < t_i \leq T,\ i = 1, 2, \ldots I$ a number of n_i additional observational resources may be deployed. We will refer to these additional observations as adaptive observations, $\mathcal{O}_i^a$, as their location may be selected in a flexible manner and it may change from one time instant to another. The observational data $\mathcal{O} = \{\mathbf{x}^o\}$ available over the assimilation

window has therefore two components $\mathcal{O} = \mathcal{O}^f \cup \mathcal{O}^a$, where $\mathcal{O}^a = \{\mathcal{O}_1^a, \mathcal{O}_2^a, \ldots, \mathcal{O}_I^a\}$ is the adaptive observational path to be determined.

4D-Var data assimilation provides an optimal estimate $\mathbf{x}_0^a$ of the true initial state $\mathbf{x}_0^t$ as the solution of the minimization problem

$$\mathcal{J}(\mathbf{x}_0) = \mathcal{J}^b + \mathcal{J}^o, \quad \mathcal{J}(\mathbf{x}_0^a) = \min_{\mathbf{x}_0} \mathcal{J}(\mathbf{x}_0) \tag{1}$$

where $\mathcal{J}^b$ is a measure of the distance of the initial state from the background estimate and $\mathcal{J}^o$ is a measure of the distance between the model trajectory and observations over the assimilation window. The reader should refer to the work of Jazwinski (1970) and Daley (1991) for a detailed description of the various assumptions used by the data assimilation techniques, including a continuum formulation and the probabilistic interpretation.

Using adaptive observations and by performing data assimilation, we aim to reduce the error of some aspect of the forecast at the verification time on the verification domain which may be expressed as

$$\mathcal{J}_v(\mathbf{x}_0) = \frac{1}{2}\langle \mathbf{P}(\mathbf{x}_v^f - \mathbf{x}_v^{ref}), \mathbf{P}(\mathbf{x}_v^f - \mathbf{x}_v^{ref})\rangle_C \tag{2}$$

where $\mathbf{x}_v^f = \mathcal{M}(\mathbf{x}_0)$, $\mathbf{x}_v^{ref}$ is the verifying analysis at t_v, and $\mathbf{P}$ is a diagonal projection operator on $\mathcal{D}_v$ satisfying $\mathbf{P}^*\mathbf{P} = \mathbf{P}^2 = \mathbf{P}$. The inner product $\langle \cdot, \cdot \rangle_C$ is defined as $\langle \mathbf{y}, \mathbf{z} \rangle_C = \langle \mathbf{y}, \mathbf{C}\mathbf{z} \rangle$ where $\mathbf{C}$ is a symmetric positive definite matrix. In practice the total energy norm is often used to measure the forecast error (2).

The adaptive observations problem is now formulated as follows: find an adaptive observational path $\mathcal{O}^a = \{\mathcal{O}_1^a, \mathcal{O}_2^a, \ldots, \mathcal{O}_I^a\}$ such that the solution $\mathbf{x}_0^a$ of the corresponding 4D-Var data assimilation (1) minimizes the forecast error expressed by the functional (2).

In previous studies only one targeting time t_i was taken into consideration ($I = 1$). Our problem formulation takes fully into account the temporal dimension of the 4D-Var scheme by considering multiple targeting instances (a.e. $I > 1$) in the assimilation window.

3 The shallow-water model

The numerical experiments and the analysis presented in this paper were performed in the twin experiments framework using a global two-dimensional shallow-water model. In spherical coordinates, the dynamical equations are written

$$\frac{\partial u}{\partial t} + \frac{1}{a\cos\theta}\left[u\frac{\partial u}{\partial \lambda} + v\cos\theta\frac{\partial u}{\partial \theta}\right] - (f + \frac{u}{a}\tan\theta)v + \frac{g}{a\cos\theta}\frac{\partial h}{\partial \lambda} = 0 \tag{3}$$

$$\frac{\partial v}{\partial t} + \frac{1}{a\cos\theta}\left[u\frac{\partial v}{\partial \lambda} + v\cos\theta\frac{\partial v}{\partial \theta}\right] + (f + \frac{u}{a}\tan\theta)u + \frac{g}{a}\frac{\partial h}{\partial \theta} = 0 \tag{4}$$

$$\frac{\partial h}{\partial t} + \frac{1}{a\cos\theta}\left[\frac{\partial}{\partial \lambda}(hu) + \frac{\partial}{\partial \theta}(hv\cos\theta)\right] = 0 \tag{5}$$

where $f = 2\Omega\sin\theta$ is the Coriolis parameter, Ω is the angular speed of the rotation of the earth, h is the height of the homogeneous atmosphere, u and v are the zonal and meridional wind components respectively, θ and λ are the latitudinal and longitudinal directions respectively, a is the radius of the earth, and g is the gravitational constant.

The software developed by Giraldo and Neta (1995) was used to implement the forward model integration. We consider a discretization on a 72×36 grid ($5^\circ \times 5^\circ$) such that the dimension of the discrete state vector $\mathbf{x} = (h, u, v)$ is 7776. The model is integrated for 24h using an explicit Turkel-Zwas scheme (Navon and de Villiers 1987, Neta et al. 1997) and a Robert filtering using a Laplacian type time-diffusion term is performed for both spatial and temporal smoothing. To maintain numerical stability, the integration time step is limited to $\Delta t = 200s$. Data obtained from a 500mb analysis valid for 00Z 16 Mar 2001 6h using the GEOS-3 model ($1.25^\circ \times 1^\circ$) was used to specify the geopotential height at the initial time t_0 and the initial velocity fields were obtained from a geostrophic approximation. The model state at the initial time and after a 24h integration are displayed in Fig. 1.

3.1 The twin experiments framework

The data assimilation procedure and the impact of the adaptive observations are analyzed using a perfect model scenario. We will assume that the initial conditions described in the previous section represent the true (reference) atmospheric state $\mathbf{x}_0^{ref}$ and the model trajectory $\mathbf{x}^{ref}(t)$ obtained during the reference run is used to provide observations. A background field is prescribed using a 5% random perturbation in the reference initial velocities. A forecast initiated at t_0 from the background estimate reveals large errors at the verification time $t_v = 24$h over the spatial domain $\mathcal{D}_v = [125°\text{E}\ 175°\text{E}]\times\ [80°\text{S}\ 40°\text{S}]$ which is thus selected as the verification domain. In Fig. 2 and Fig. 3 we show the errors in the background field and the 24h forecast respectively, evaluated in the total energy norm

$$\langle \delta\mathbf{x}(\lambda,\theta), \delta\mathbf{x}(\lambda,\theta)\rangle = \frac{1}{2}\left((\delta u)^2 + (\delta v)^2\right) + \frac{g}{h_0}(\delta h)^2 \tag{6}$$

where $\delta\mathbf{x}(\lambda,\theta) = \mathbf{x}(\lambda,\theta) - \mathbf{x}^{ref}(\lambda,\theta)$.

4D-Var data assimilation is performed in the assimilation window $[0-6]$h and we assume that routine observations are available at t=6h only on a coarse $20°\times 20°$ mesh grid. The error in the forecast initiated from the analysis obtained with the data assimilation using routine observations is shown in Fig. 4. We notice that the overall quality of the forecast is improved over the entire domain. However, the forecast error over the domain of interest, $\mathcal{D}_v$, remains relatively large. To further improve the forecast over $\mathcal{D}_v$, we assume that each hour in the interval $[0-6]$h five adaptive observations may be taken and their optimal location must be determined by an appropriate targeting procedure. In the next section we review two traditional adjoint-based targeting methods: the singular vectors and the adjoint sensitivity.

4 Singular vectors and adjoint sensitivity

Implementation of the adjoint-based targeting methods relies on the linearization of the nonlinear forecast model. The intimate relationship between the adjoint (gradient) sensitivity and singular vectors is discussed by Rabier et al. (1996). If we consider a perturbation $\delta\mathbf{x}_i$ of the model state at t_i then, to first order approximation, the induced perturbation at t_v is expressed as

$$\delta\mathbf{x}_v = \mathcal{M}(\mathbf{x}_i + \delta\mathbf{x}_i) - \mathcal{M}(\mathbf{x}_i) \approx \mathbf{L}(t_i, t_v)\delta\mathbf{x}_i \tag{7}$$

where $\mathbf{L}(t_i, t_v)$ is the resolvent of the tangent linear model in the optimization interval $t_v - t_i$. On the tangent phase space we consider an inner product

$$\langle \delta\mathbf{x}, \delta\mathbf{y} \rangle_C = \langle \delta\mathbf{x}, \mathbf{C}\delta\mathbf{y} \rangle \tag{8}$$

where $\mathbf{C}$ is a symmetric positive definite matrix (usually taken to be diagonal), and $\langle \cdot, \cdot \rangle$ is the Euclidean inner product. The adjoint operator of $\mathbf{L}$ in $\langle \cdot, \cdot \rangle_C$ is defined as:

$$\langle \mathbf{L}^{*C}\delta\mathbf{x}, \delta\mathbf{y} \rangle_C = \langle \delta\mathbf{x}, \mathbf{L}\delta\mathbf{y} \rangle_C \tag{9}$$

such that $\mathbf{L}^{*C} = \mathbf{C}^{-1}\mathbf{L}^*\mathbf{C}$, where $\mathbf{L}^*$ is the adjoint operator of $\mathbf{L}$ in $\langle \cdot, \cdot \rangle$.

4.1 The singular vectors approach

The singular vectors approach to targeting observations (Palmer et al. 1998, Buizza and Montani 1999) searches for the directions where errors in the state vector at the targeting time will propagate most at the verification time on the verification domain. From (9) it follows that

$$\|\delta\mathbf{x}(t_v)\|_C = \langle \delta\mathbf{x}(t_i), \mathbf{L}^{*C}\mathbf{L}\delta\mathbf{x}(t_i) \rangle_C \tag{10}$$

such that the directions characterized by maximum relative growth $\|\delta\mathbf{x}(t_v)\|_C / \|\delta\mathbf{x}(t_i)\|_C$ are the singular vectors $\nu_j(t_i)$

$$\mathbf{L}^{*C}\mathbf{L}\nu_j(t_i) = \sigma_j^2 \nu_j(t_i) \tag{11}$$

associated with the largest singular values σ_j.

The singular vectors (11) depend on the C-norm selection. Palmer et al. (1998) show that the analysis error covariance metric (AECM) is an optimal choice to improve the forecast skill. The total energy metric offers a reasonable first order estimate of the AECM (Palmer et al. 1998) and is often used to facilitate the practical implementation.

If $\mathbf{P}$ denotes the projection operator on $\mathcal{D}_v$, the singular value problem

$$\left[\mathbf{C}^{\frac{1}{2}}\mathbf{P}\mathbf{L}\mathbf{C}^{-\frac{1}{2}}\right]^{*}\mathbf{C}^{\frac{1}{2}}\mathbf{P}\mathbf{L}\mathbf{C}^{-\frac{1}{2}}\mu_j = \sigma^2\mu_j \tag{12}$$

$$\nu_j = \mathbf{C}^{-\frac{1}{2}}\mu_j \tag{13}$$

must be solved in the optimization interval $t_v - t_i$.

Iterative solvers (see e.g. ARPACK package, Lehoucq et al. 1998) may be used to evaluate the singular values and the associated singular vectors. For large-scale atmospheric models this is an intensive computational process and in practice only 4 to 10 leading singular vectors are used to define the target area as we explain next.

4.1.1 Target area definition using N leading singular vectors

To identify the target area at the targeting time t_i we follow the approach of Buizza and Montani (1999). Consider the first N leading singular vectors $\nu_j, j = 1, 2, \ldots N$ at t_i with unit C-norm, $\|\nu_j\|_C = 1, j = 1, 2, \ldots N$ and let $f_j^C(\lambda, \theta)$ denote the value of the C-norm of ν_j at grid point (λ, θ) (e.g. total energy norm at (λ, θ)). A sensitivity function is defined as

$$F_N^C(\lambda, \theta) = \sum_{j=1}^{N}\left(\frac{\sigma_j}{\sigma_1}\right) f_j^C(\lambda, \theta) \tag{14}$$

Additional observations taken at t_i at the locations where the sensitivity field (14) is maximal are believed to be of significant benefit for the forecast improvement. The target area is defined as

$$\mathcal{D}_i = \{(\lambda, \theta) | F_N^C(\lambda, \theta) \geq 0.5 F_{MAX}\}; \qquad F_{MAX} = \max_{(\lambda,\theta)} F_N^C(\lambda, \theta) \tag{15}$$

and adaptive observations locations at t_i are selected as the first n_i locations (λ, θ) where $F_N^C(\lambda, \theta)$ attains the largest values.

The computational cost of implementing targeting methods using singular vectors is significantly increased when multiple targeting instants are considered since for each $t_i, i = 1, 2, \ldots I$ a new set of singular vectors must be computed.

4.2 The adjoint sensitivity approach

In the adjoint sensitivity approach adaptive observations are selected using the gradient of a functional $\mathcal{J}^v$ defined in terms of the forecast at the verification time. Ideally, we would like to evaluate the sensitivity of the forecast error (2) with respect to the model state at the targeting time. A large sensitivity value indicates that small variations in the model state will have a significant impact on the forecast at the verification time. However, since the forecast error at t_v is not known at the initial time, for practical applications (e.g. flight planning) the functional $\mathcal{J}^v$ must be based on the forecast alone. For theoretical or 'a posteriori' studies, we may consider $\mathcal{J}^v$ to be the cost functional (2) representing the forecast error at t_v. The sensitivity field is defined as

$$F_v(\lambda, \theta) = \|\nabla \mathcal{J}_v^C(\lambda, \theta)\|_C \tag{16}$$

where $\nabla \mathcal{J}_v^C$ is the gradient of the verification functional. Corresponding to (2) we have

$$\nabla \mathcal{J}_v^C(\mathbf{x}_i) = \mathbf{L}^{*C}\mathbf{P}(\mathbf{x}_v^f - \mathbf{x}_v^{ref}) \tag{17}$$

Adaptive observations at t_i are deployed at the first n_i locations (λ, θ) where $F_v(\lambda, \theta)$ has largest values. Identification of the target area at distinct instants in time proceeds backward from t_I to t_1 and an efficient evaluation of all $\nabla \mathcal{J}_v^C(\mathbf{x}_i), i = 1, 2, \ldots I$ is obtained through a single adjoint model integration. The adjoint sensitivity method may be therefore implemented at a reduced computational cost even in the case when multiple targeting instants are considered.

5 Interactive adaptive observations

Baker and Daley (2000) noticed that traditional targeting methods based on the 'a priori' evaluation of a sensitivity field such as (14) and (16) are completely ignorant of the characteristics of the data assimilation systems. Using the adaptive methods described in the previous section optimal adaptive observations at t_i have been determined assuming that these are *the only* available observations. Since 4D-Var data assimilation takes into consideration *all* observations available in the assimilation window, the interaction between observations must be considered by the targeting procedure. In particular, the following question should be addressed: If individually each of $\mathcal{O}_i^a$ at $t_i, i = 1, 2, \ldots, I$ is an optimal adaptive observations set, is $\mathcal{O}^a = \{\mathcal{O}_1^a, \mathcal{O}_2^a, \ldots, \mathcal{O}_I^a\}$ still optimal? Bishop (2000) shows with a simple example that an attempt to globally search for an optimal solution from the set of all feasible adaptive observations paths may easily lead to a problem which is computationally impractical. Therefore, even for practical applications of moderate complexity, a serial observations processing must be considered.

The new adjoint sensitivity approach we describe in this section takes into consideration the interaction between adaptive observations at distinct instants in time and the interaction with routine observations. The selection algorithms proceeds backward in time and adaptive observations $\mathcal{O}_i^a$ are selected in a sequential manner. A periodic update of the sensitivity field at t_i is performed to account for all observations already located at t_{i+1}. Denote by

$$\mathcal{O}_{i+1} = \mathcal{O}^f \cup \mathcal{O}_I^a \cup \ldots \cup \mathcal{O}_{i+1}^a \tag{18}$$

the set of all observations already located at time t_{i+1} and consider $\mathcal{J}_{\mathcal{O}_{i+1}}(\mathbf{x}_i)$ the cost functional (1) restricted to the observational set $\mathcal{O}_{i+1}$ as a function $\mathbf{x}_i$.

We introduce a new sensitivity field associated to the observations set $\mathcal{O}_{i+1}$

$$F_i(\lambda, \theta) = \|\nabla \mathcal{J}_{\mathcal{O}_{i+1}}(\lambda, \theta)\|_C \tag{19}$$

and update the sensitivity field F_v at t_i according to

$$F_v(\lambda,\theta) = F_v(\lambda,\theta)\left(1+\alpha\frac{F_i(\lambda,\theta)}{F_v(\lambda,\theta)}\right)^{-1} \tag{20}$$

The updated sensitivity field is inversely proportional to the relative value of the sensitivity field provided by the set of observations that have been already located. Optimal sites for deploying adaptive observations at t_i are now selected at the locations where the sensitivity field (20) has the largest magnitude. Therefore, new observations at t_i are located in regions where the sensitivity of $\mathcal{J}_v$ to the model state is large *and* little additional information may be obtained from *all previously located* observations. The interaction between observations is controlled by the weight coefficient $\alpha > 0$ which reflects our confidence in the previously selected observations (e.g. observational errors).

The sensitivity field F_i may be evaluated at once for all $i = I, I-1, \ldots, 1$ by periodically updating the observational set (18) during the adjoint model integration. The additional computational cost is roughly given by the computational cost of a backward integration in the assimilation window $[t_0, T]$. In practice the length assimilation window is much smaller than the length of the time interval $[t_0, t_v]$ such that the computational overhead required by the update (19) - (20) is relatively small compared to the evaluation of the sensitivity field (16). The benefits of the new approach to targeting observations are presented next in a comparative analysis with both the adjoint sensitivity and singular vectors methods.

Remark. Since the sensitivity field (19) depends on the observations, the update (19) - (20) may be used only for 'a posteriori' targeting applications. However, the method may be easily extended for 'a priori' estimates, by defining the functional $\mathcal{J}_{\mathcal{O}_{i+1}}(\mathbf{x}_i)$ only in terms of the forecast at the locations (λ,θ) determined by $\mathcal{O}_{i+1}$, in a similar manner as $\mathcal{J}_v$. This approach was presented in the recent work of Daescu and Carmichael (2002).

6 Numerical experiments

In this section targeting strategies using the leading total energy singular vectors (TESV), adjoint sensitivity (AS), and adjoint sensitivity with interactions between observations (IAS) are analyzed for the shallow-water model and the experimental settings described in Section 3. We assume that each hour in the assimilation window $[0, 6\text{h}]$ five adaptive observations must be selected using an appropriate targeting strategy. A comparative performance analysis is presented for two different scenarios: In the first experiment (E1) we assume that the adaptive observations are the only observations available to the data assimilation process ($\mathcal{O}^f = \emptyset$). In the second experiment (E2) we assume that routine observations are also available on a $20^\circ \times 20^\circ$ coarser mesh grid. For each experiment and for each of the targeting methods a new data assimilation procedure is performed using the quasi-Newton limited memory BFGS minimization algorithm (Liu and Nocedal 1989). The minimization proceeds until the cost functional is reduced to 0.1% of its initial value. For each targeting method, during the minimization process of the cost functional $\mathcal{J}$ (over the entire domain) which provides the initial condition $\mathbf{x}_0^a$, we also monitor the evolution of the normalized forecast error reduction $\mathcal{J}_v(\mathbf{x}_0^a)/\mathcal{J}_v(\mathbf{x}_0)$ at $t_v = 24\text{h}$ over the verification domain $\mathcal{D}_v = [125^\circ\text{E}\ 175^\circ\text{E}]\times\ [80^\circ\text{S}\ 40^\circ\text{S}]$. The total energy norm is used to define the inner product $\langle\cdot,\cdot\rangle_C$ and to quantify the forecast error (2) at t_v.

To implement the AS and IAS methods we used the gradient fields F_v associated to the verification functional (2) ('a posteriori' targeting). To implement the TESV method, 10 leading singular values and their associated singular vectors were computed at each targeting instant t_i using the ARPACK package (Lehoucq et al. 1998). The evolution of the first singular vector in 500hPa geopotential height field for the optimization interval [t, 24h] with t= 0h, 2h, 4h, 6h is shown in Fig. 5. Similarly, in Fig. 6 we show the time evolution of the first singular vector in zonal wind field. The adjoint model associated with the forward model discretization was generated using the automatic adjoint compiler TAMC (Giering and Kaminski 1998). The validity of the linear model approximation

(7) in the interval [0, 24h] was verified by comparing nonlinearly evolved perturbations (control minus perturbed experiment) with a perturbation evolved using the tangent operator.

6.1 A comparative analysis of targeting methods

We begin our analysis by presenting the results obtained for the experiment E1 when only adaptive observations are provided to the data assimilation. The evolution of the sensitivity field obtained with the adjoint sensitivity (AS) method is shown in Fig. 7 for t_i = 0h, 2h, 4h, 6h. The location of the adaptive observations (marked with $'\triangle'$ in Fig. 7) corresponds to the grid points where the sensitivity field has the largest magnitude.

The dynamics of the sensitivity field is significantly changed when the interaction between the observations is taken into consideration as we show in Fig. 8 for the IAS targeting method. Adaptive observations using adjoint sensitivity with interaction between observations (IAS) are marked in Fig. 8 with $'\square'$. Locations marked with $'\triangle'$ in Fig. 8 were selected also by the previous approach (AS). Since the selection of the adaptive observations proceeds backward in time, t_I = 6h is the first targeting instant. At this time no observations were previously located such that the sensitivity fields are identical and both AS and IAS methods selected the same set of observations. To identify new locations at the following targeting instants, the IAS method takes into consideration the influence of all observations already located. From Fig. 7 and Fig. 8 we notice that the periodical update of the sensitivity field results in less spatial clustering for the adaptive observations. The IAS method searches to identify regions where the magnitude of the sensitivity field is large, conditioned by the information accumulated from previously located observations.

The evolution of the sensitivity field corresponding to the total energy singular vectors method is shown in Fig. 9, and the location of the adaptive observations is marked with $'\circ'$. For each targeting method, the distribution of the forecast error at the verification time over the verification domain after data assimilation takes place is shown in the

total energy norm in Fig. 10. The forecast error using the background estimate as initial conditions is also displayed in Fig. 10. At each iteration during the minimization process of the cost functional $\mathcal{J}$ we monitor the forecast improvement using targeted observations by evaluating the ratio $\mathcal{J}_v(\mathbf{x}_0^a)/\mathcal{J}_v(\mathbf{x}_0)$. The results displayed in Fig. 11 show that the targeting method using interactive adaptive observations outperforms the adjoint sensitivity as well as the singular vectors targeting methods.

Next we analyze the forecast improvement for the second scenario, E2, when both routine and adaptive observations are provided to the data assimilation. The benefits of using adaptive observations are evaluated by comparison with an assimilation procedure using only routine observations. Four data assimilation experiments were performed with observations provided as follows: fixed observations only, fixed and adaptive observations using singular vectors, fixed and adaptive observations using adjoint sensitivity, fixed and adaptive observations using adjoint sensitivity with interaction between observations. For each experiment, the minimization process and the forecast error reduction $\mathcal{J}_v(\mathbf{x}_0^a)/\mathcal{J}_v(\mathbf{x}_0)$ during the minimization of the corresponding cost functional $\mathcal{J}$ are shown in Fig. 12. The distribution of the forecast error at the verification time over the verification domain is displayed in Fig. 13.

The potential forecast improvement using adaptive observations is limited by various factors such as the accuracy of the background estimate, the configuration of the existing observational network, and the number of additional observational resources allocated. In Fig. 12 it can be seen that the adaptive method using the interaction between observations still provided the best forecast over $\mathcal{D}_v$, but there is only little improvement as compared to the adjoint sensitivity method.

Remark. One should notice that by using adaptive observations we only attempt to improve the forecast over a given sub-domain at a given future time. In Fig. 14 we show the distribution of the forecast error at 24h over the entire domain after data assimilation using fixed and interactive adaptive observations takes place. By comparison with Fig.

4, it can be seen that adaptive observations have significant benefits on the forecast over the verification domain $\mathcal{D}_v$ = [125°E 175°E]× [80°S 40°S], and little or no forecast improvement is observed outside this region.

7 Conclusions and further research

In this study the adaptive observations problem is presented in the context of 4D-Var data assimilation. It is emphasized that to fully account for the temporal dimension of the 4D-Var scheme, multiple targeting instants must be considered in the assimilation window. Our work represents a first step in the design of optimal sampling strategies for time distributed adaptive observations. In particular, it is shown that the interaction between targeted observations taken at distinct instants in time has a significant impact on the efficiency of the adaptive strategies.

A new adjoint sensitivity approach for adaptive observations is proposed which takes into consideration the interaction between adaptive observations at distinct instants in time and their interaction with routine observations. The main difference between the proposed method and the traditional adjoint sensitivity approach consists in the dynamic update of the sensitivity field associated with the verification functional. To perform this update, a new sensitivity field is used to quantify the information accumulated at the targeting time from all previously located observations. A simple interaction mechanism is designed such that new adaptive observations are located in regions where the sensitivity of the forecast to the model state is large and little additional information may be obtained from all previously located observations. The additional computational cost is given by a backward integration of the adjoint model in the assimilation window such that the method is feasible to implement for large scale applications. No claim is made that the proposed approach provides an optimal adaptive observational path among all feasible sets of observations. However, our analysis presented for a global 2D shallow-water model shows that the new targeting method outperforms traditional targeting methods such as

the total energy singular vectors and the adjoint sensitivity.

Given the potential impact to improve the models forecasts and the multitude of practical applications, significant research remains do be done to develop optimal adaptive observations techniques. Our future research will focus on the implementation of targeting methods using interactive adjoint sensitivity fields for comprehensive operational atmospheric models. A rigorous theoretical framework to account for time distributed adaptive observations remains to be formulated. We will also investigate the application of interactive sensitivity fields to targeting methods using singular vectors and ensemble forecasts. The sensitivity to observations technique proposed by Baker and Daley (2000) may be extended to the 4D-Var data assimilation to analyze the interaction between the existing observational network, the background estimate of the model state, and adaptive observations.

Acknowledgements

The authors acknowledge the support from the School of Computational Science and Information Technology, Florida State University. The second author acknowledges the support from the NSF grant number ATM-0201808 managed by Dr. Linda Peng whom he would like to thank for her support.

References

Baker NL, Daley R (2000) Observation and background adjoint sensitivity in the adaptive observation-targeting problem. *Q.J.R. Meteorol. Soc.*, **126**, 1431-1454

Bergot T (2001) Influence of the assimilation scheme on the efficiency of adaptive observations. *Q.J.R. Meteorol. Soc.*, **127**, 635-660.

Berliner LM, Lu Z-Q, Snyder C (1999) Statistical design for adaptive weather observations. *J. Atmos. Sci.*, **56**, 2536-2552

Bishop CH (2000) Estimation theory and adaptive observing techniques. Submitted to *Q.J.R. Meteorol. Soc.*

Bishop CH, Toth Z (1999) Ensemble transformation and adaptive observations. *J. Atmos. Sci.*, **56**, 1748-1765

Bishop CH, Etherton BJ, Majumdar SJ (2001) Adaptive sampling with the ensemble transform Kalman filter. Part I: Theoretical aspects. *Mon. Weather Rev.* **129**, 420-436

Buizza R, Montani A (1999) Targeted observations using singular vectors.*J. Atmos. Sci.* **56**, 2965-2985

Courtier P, Thepaud JN, Hollingsworth A (1994) A strategy of operational implementation of 4D-Var using an incremental approach. *Q.J.R. Meteorol. Soc.*, **120**, 1367-1388

Daescu DN, Carmichael GR (2002) An adjoint sensitivity method for the adaptive location of the observations in air quality modeling. Submitted to *J. Atmos. Sci.*

Daley R (1991) *Atmospheric Data Analysis*. Cambridge University Press, 457pp.

Doerenbecher A, Bergot T (2001) Sensitivity to observations applied to FASTEX cases. *Nonlinear Processes in Geophys.*, **8**, 467-481

Giering R, Kaminski T (1998) Recipes for adjoint code construction. *ACM Trans. Math. Software*, **24** (4), 437-474

Giraldo FX, Neta B (1995) Software for the staggered and unstaggered Turkel-Zwas schemes for the shallow water equations on the sphere. NPS-MA-95-008, Technical Report Naval Postgraduate School, Monterey, CA.

Hansen JA, Smith LA (2000) The role of operational constraints in selecting supplementary observations. *J. Atmos. Sci.*, v. **57**, no. 17, 2859-2871.

Jazwinski AH (1970) *Stochastic Processes and Filtering Theory.* Academic Press, 376pp

Joly A, and Coauthors (1997) The Fronts and Atlantic Storm-Track Experiment (FASTEX): Scientific objectives and experimental design. *Bull. Amer. Meteorol. Soc.*, **78**, 1917-1940

Kalnay E, Park SK, Pu Z-X, Gao J (2000) Applications of the quasi-inverse method to data assimilation. *Mon. Weather Rev.*, **128**, 864-875

Langland R, Rohaly G (1996) Adjoint-based targeting of observations for FASTEX cyclones. *Preprints, Seventh Conf. on Mesoscale Process, Reading, United Kingdom, Amer. Meteor. Soc.*, 369-371

Langland RH, Toth Z, Gelaro R, Szunyogh I, Shapiro MA, Majumdar SJ, Morss RE, Rohaly GD, Velden C, Bond N, and Bishop CH (1999) The North Pacific experiment (NORPEX-98): Targeted observations for improved North American weather forecasts. *Bull. Amer. Meteorol. Soc.*, **80**, 1363-1384

Lehoucq RB, Sorensen DC, Yang C (1998) *ARPACK User's Guide: Solution of Large-Scale Eigenvalue Problems with Implicitly Restarted Arnoldi Methods.* Software, Environments, and Tools, Vol. 6, SIAM, 160pp

Leutbecher M, Barkmeijer J, Palmer TN, Thorpe AJ (2002) Potential improvement of forecasts of two severe storms using targeted observations. To appear in *Q.J.R. Meteorol. Soc.*

Liu, DC, Nocedal, J (1989) On the limited memory BFGS method for large scale minimization. *Math. Prog.,* **45**, 503-528.

Lorenz EN, Emanuel KA (1998) Optimal sites for supplementary weather observations: Simulation with a small model. *J. Atmos. Sci.*, **55**, 399-414

Majumdar SJ, Bishop CH, Buizza R, Gelaro R (2002) A comparison of PSU-NCEP Ensemble Transform Kalman Filter Targeting Guidance with ECMWF and NRL Singular

Vector Guidance. To appear in *Q.J.R. Meteorol. Soc.*

Morss RE, Emanuel KA, Snyder C (2001) Idealized adaptive observation strategies for improving numerical weather prediction. *J. Atmos. Sci.*, **58** 210-234.

Navon IM, de Villiers R (1987) The application of the Turkel-Zwas explicit large time step scheme to a hemispheric barotropic model with constraint restoration. *Mon. Weather Rev.*, **115**, No. 5, 1036-1051.

Neta B, Giraldo FX, Navon IM (1997) Analysis of the Turkel-Zwas scheme for the two-dimensional shallow water equations in spherical coordinates. J. Comput. Phys., **133** , No. 1, 102-112

Palmer TN, Gelaro R, Barkmeijer J, and Buizza R (1998) Singular vectors, metrics, and adaptive observations. *J. Atmos. Sci.*, **55**, 633-653

Pu Z-X, Kalnay E (2000) Targeting observations with the quasi-inverse linear and adjoint NCEP global models: performance during FASTEX. *QJR Meteorol. Soc.*, **125**, 3329-3337

Rabier F, Klinker E, Courtier P, and Hollingsworth A (1996) Sensitivity of forecast errors to initial conditions. *Q.J.R. Meteorol. Soc.*, **122**, 121-150.

Szunyogh I, Toth Z, Morss RE, Majumdar SJ, Etherton BJ, Bishop CH (2000) The effect of targeted dropsonde observations during the 1999 winter storm reconnaissance program. *Mon. Weather Rev.* **128**, 3520-3537

Figure Captions

Figure 1. The configuration of the model state for the reference run ($\mathbf{x}_0^{ref}$): 500hPa geopotential height and velocities field at the initial time t=0h and after a 24h forecast.

Figure 2. Distribution of the error $\mathbf{x}^b - \mathbf{x}_0^{ref}$ in the background estimate of the initial model state. Isopleths of the magnitude of are shown in the total energy norm.

Figure 3. Distribution of the forecast error at t=24h using the background estimate as the initial condition. Isopleths of the magnitude of are shown in the total energy norm. The largest forecast error is observed over the region $\mathcal{D}_v$ = [125°E 175°E]× [80°S 40°S] which is thus selected as the verification domain.

Figure 4. Distribution of the forecast error in total energy norm at the verification time when data assimilation is performed with observations from fixed locations only ($20^\circ \times 20^\circ$ coarse grid). The verification domain $\mathcal{D}_v$ = [125°E 175°E]× [80°S 40°S] is shown with solid line.

Figure 5. Time evolution of the first singular vector in 500hPa geopotential height field for the optimization interval [t_i, 24h]. Results shown for t_i = 0h, 2h, 4h, 6h.

Figure 6. Time evolution of the first singular vector in zonal wind field for the optimization interval [t_i, 24h]. Results shown for t_i = 0h, 2h, 4h, 6h.

Figure 7. Time evolution of the sensitivity field corresponding to the adjoint sensitivity

method (AS). Results shown for t_i = 0h, 2h, 4h, 6h. The location of the adaptive observations at t_i is marked with $'\triangle'$ and corresponds to the grid points where the sensitivity field has the largest magnitude.

Figure 8. Time evolution of the sensitivity field corresponding to the adjoint sensitivity method with interaction between observations (IAS). Results shown for t_i = 0h, 2h, 4h, 6h. The location of the adaptive observations selected by the IAS method at t_i is marked with $'\square'$. Locations marked with $'\triangle'$ were also selected by the AS method (Fig. 7).

Figure 9. Time evolution of the sensitivity field and adaptive observations location (marked with $'\circ'$) using the leading singular vectors method (TESV). Results shown for t_i = 0h, 2h, 4h, 6h.

Figure 10. Distribution of the forecast error at the verification time over the verification domain when data assimilation is performed using adaptive observations only. For reference, the error in the forecast initiated from the background estimate is also displayed. Isopleths of the magnitude are shown in the total energy norm.

Figure 11. Top: The minimization of the cost functional $\mathcal{J}$ when only adaptive observations corresponding to TESV, AS, and IAS targeting methods are assimilated. Normalized values are shown on a logarithmic scale. Bottom: During the iterative process, for each targeting method the forecast error reduction at the verification time over $\mathcal{D}_v$ is quantified by evaluating the ratio $\mathcal{J}_v(\mathbf{x}_0^a)/\mathcal{J}_v(\mathbf{x}_0)$.

Figure 12. Top: The minimization of the cost functional $\mathcal{J}$ when both routine and adaptive observations provided by the TESV, AS, and IAS targeting methods respectively, are

assimilated. Normalized values are shown on a logarithmic scale. Bottom: During the iterative process, for each targeting method the forecast error reduction at the verification time over $\mathcal{D}_v$ is quantified by evaluating the ratio $\mathcal{J}_v(\mathbf{x}_0^a)/\mathcal{J}_v(\mathbf{x}_0)$. For reference, the results obtained using routine observations only are also displayed.

Figure 13. Distribution of the forecast error at the verification time over the verification domain when data assimilation is performed using both routine and adaptive observations provided by the TESV, AS, and IAS targeting methods, respectively. For reference, the results obtained using routine observations only are also displayed.

Figure 14. Distribution of the forecast error in total energy norm at the verification time when data assimilation is performed with routine and adaptive observations provided by the IAS targeting method. Significant forecast improvement may be observed over the verification domain (see also Fig. 3 and Fig. 4).

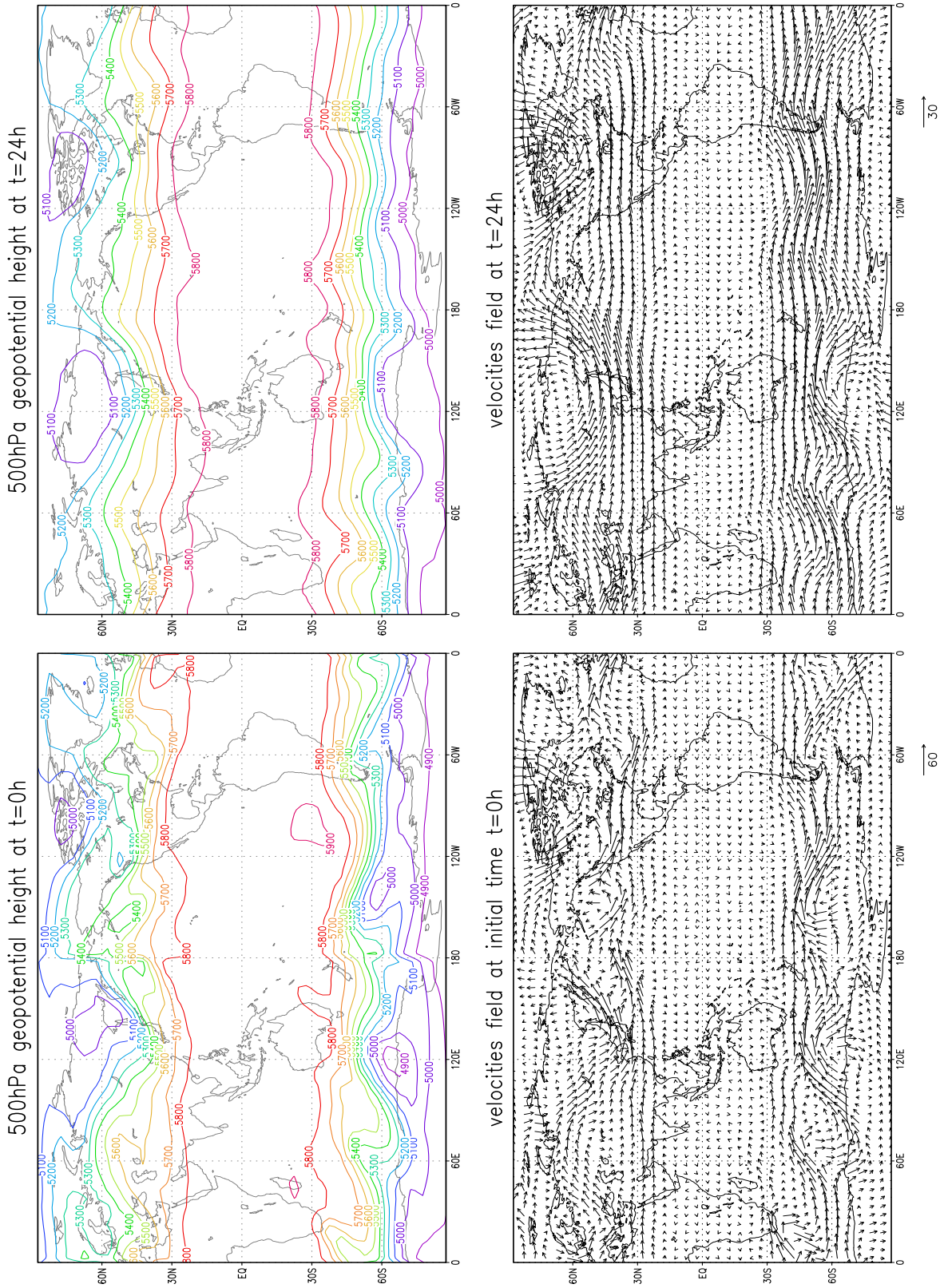
500hPa geopotential height at t=0h
500hPa geopotential height at t=24h
velocities field at initial time t=0h
velocities field at t=24h
60
30

Figure 1:

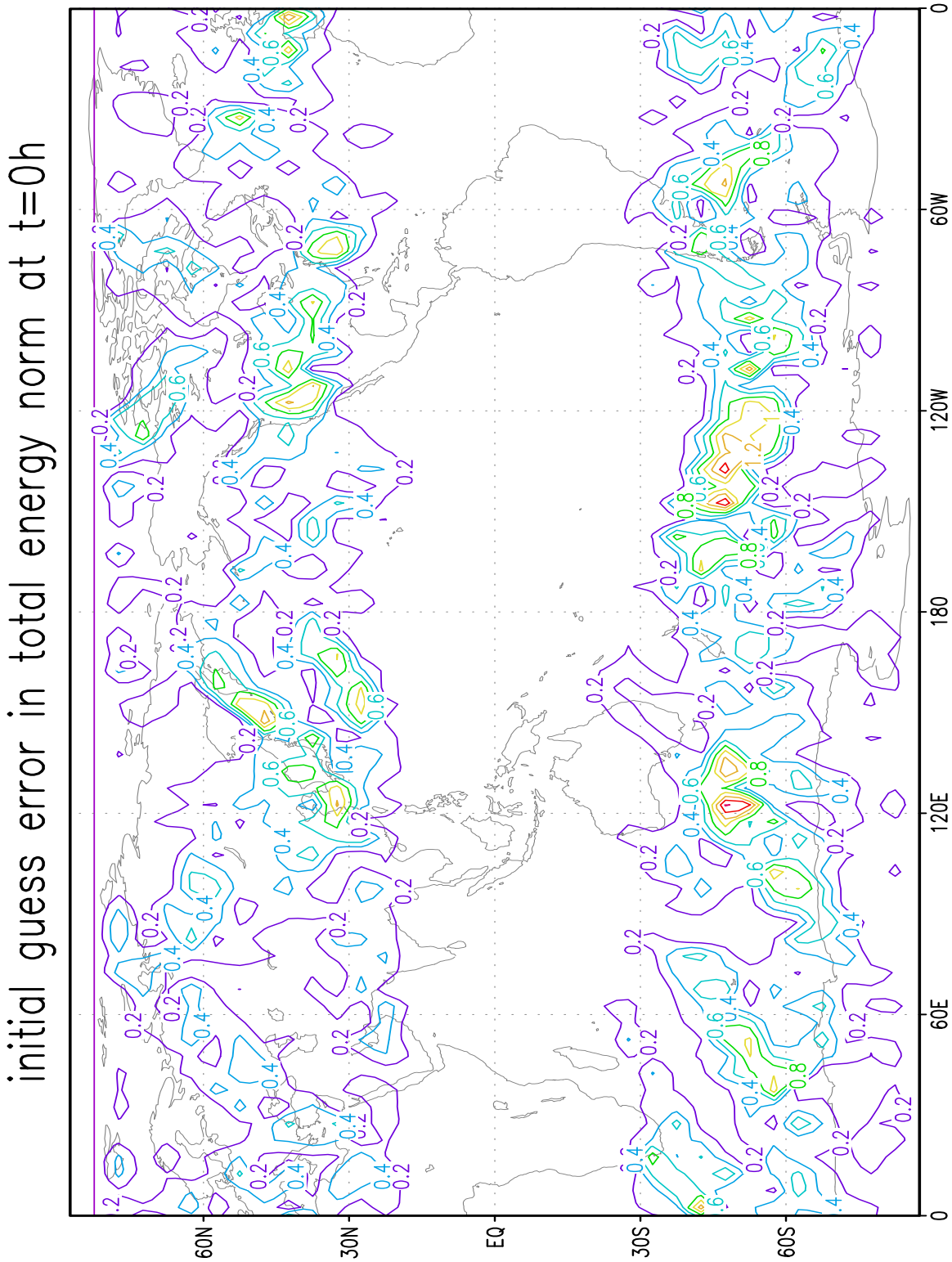
initial guess error in total energy norm at t=0h
60N
30N
EQ
30S
60S
0
60E
120E
180
120W
60W
0

Figure 2:

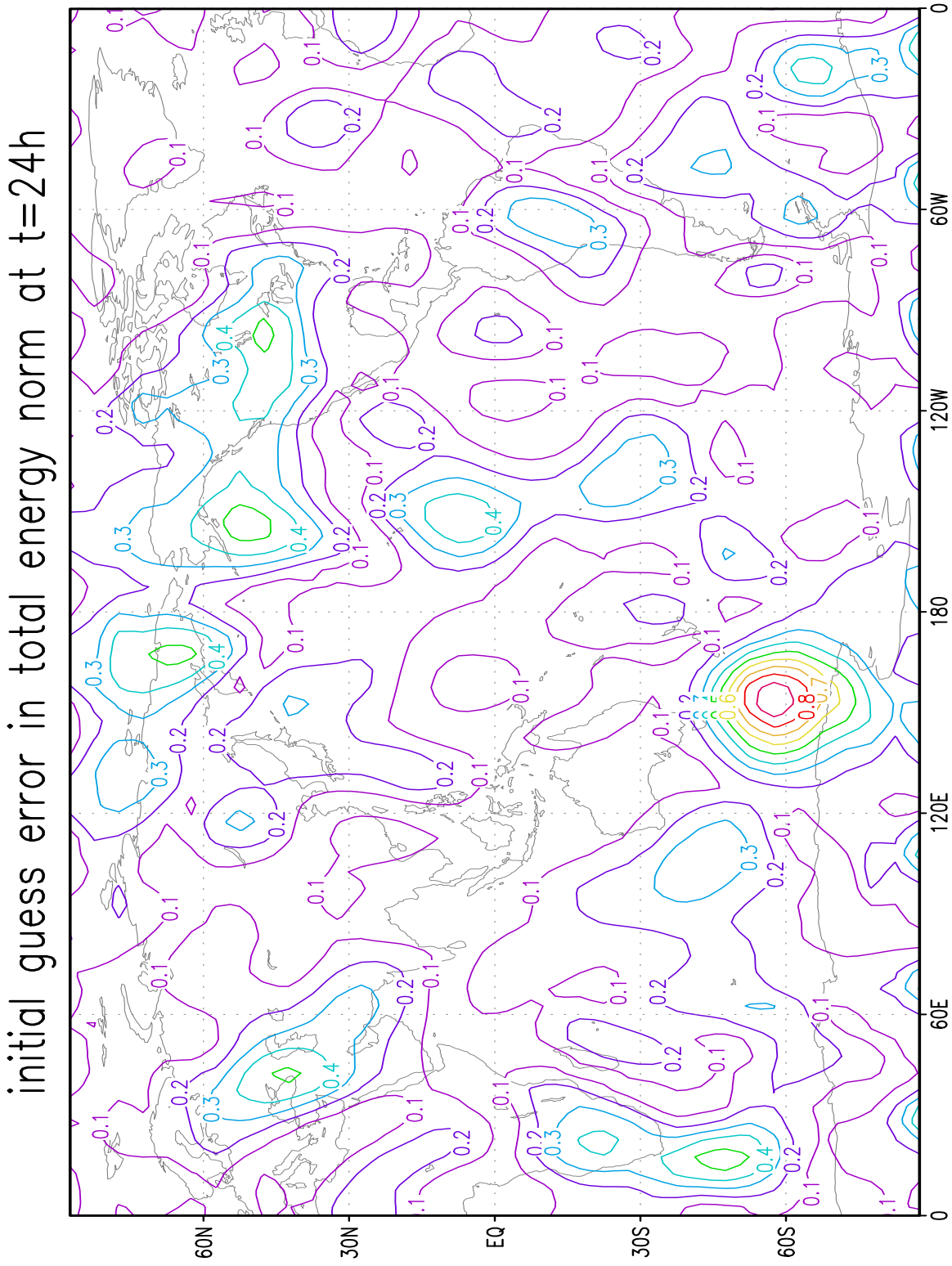
initial guess error in total energy norm at t=24h
60N
30N
EQ
30S
60S
0
60E
120E
180
120W
60W
0

Figure 3:

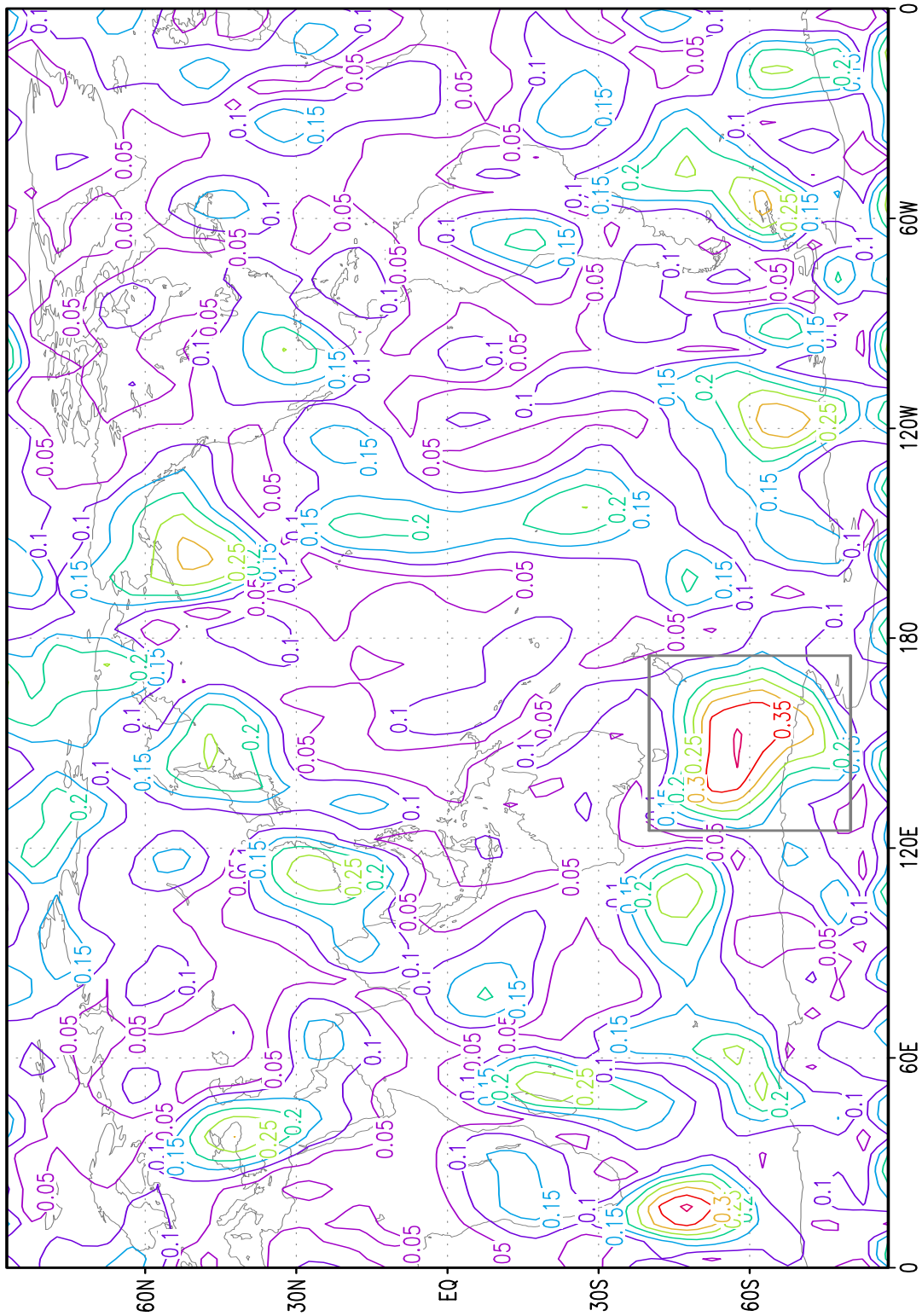
error (t.e. norm) of 24h forecast with fixed obs only
60N
30N
EQ
30S
60S
0
60E
120E
180
120W
60W
0

Figure 4:

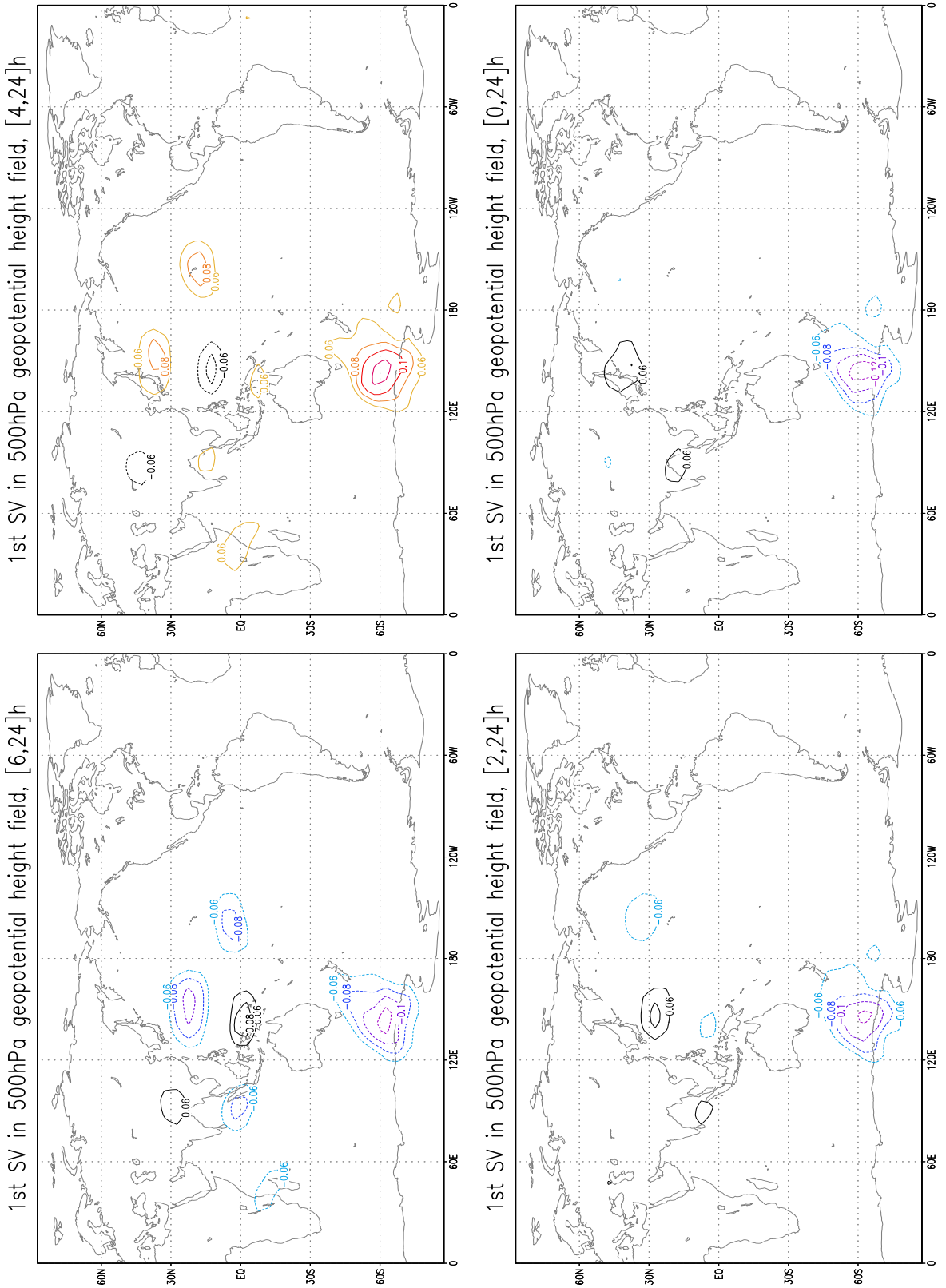
1st SV in 500hPa geopotential height field, [4,24]h
1st SV in 500hPa geopotential height field, [0,24]h
1st SV in 500hPa geopotential height field, [6,24]h
1st SV in 500hPa geopotential height field, [2,24]h
60N
30N
EQ
30S
60S
0
60E
120E
180
120W
60W

Figure 5:

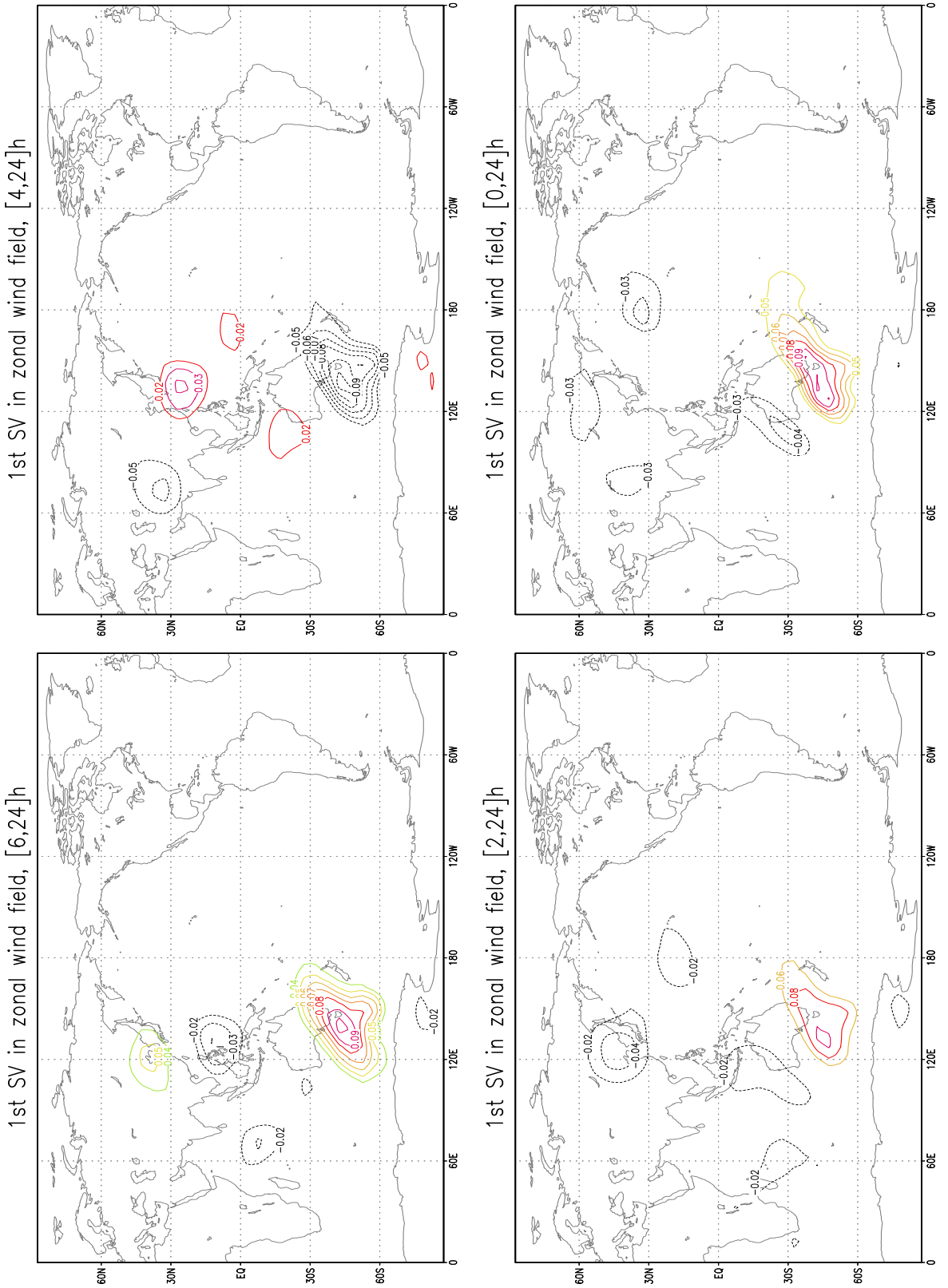
1st SV in zonal wind field, [4,24]h
1st SV in zonal wind field, [0,24]h
1st SV in zonal wind field, [6,24]h
1st SV in zonal wind field, [2,24]h
60N
30N
EQ
30S
60S
0
60E
120E
180
120W
60W

Figure 6:

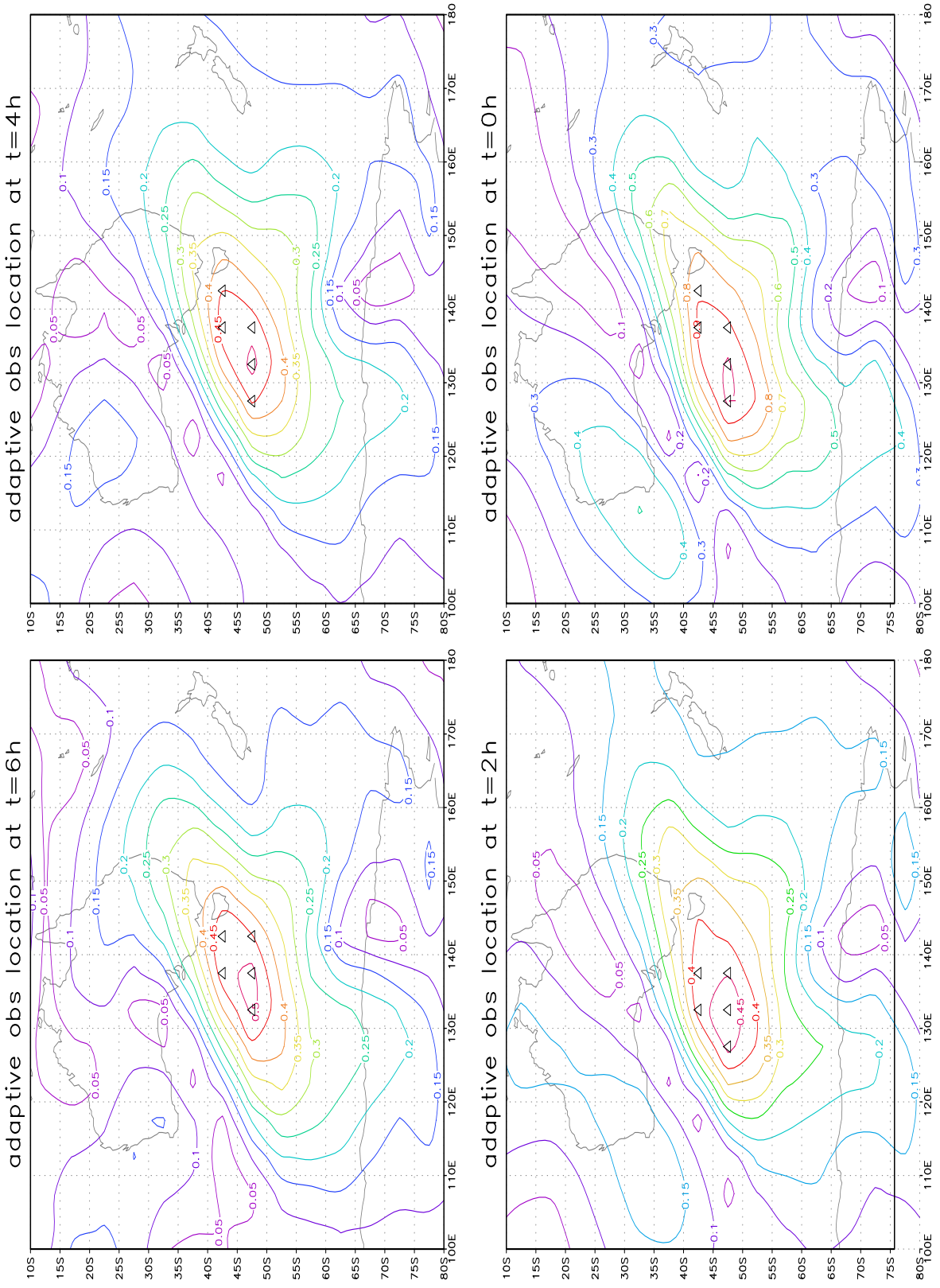
adaptive obs location at t=4h
adaptive obs location at t=6h
adaptive obs location at t=0h
adaptive obs location at t=2h

Figure 7:

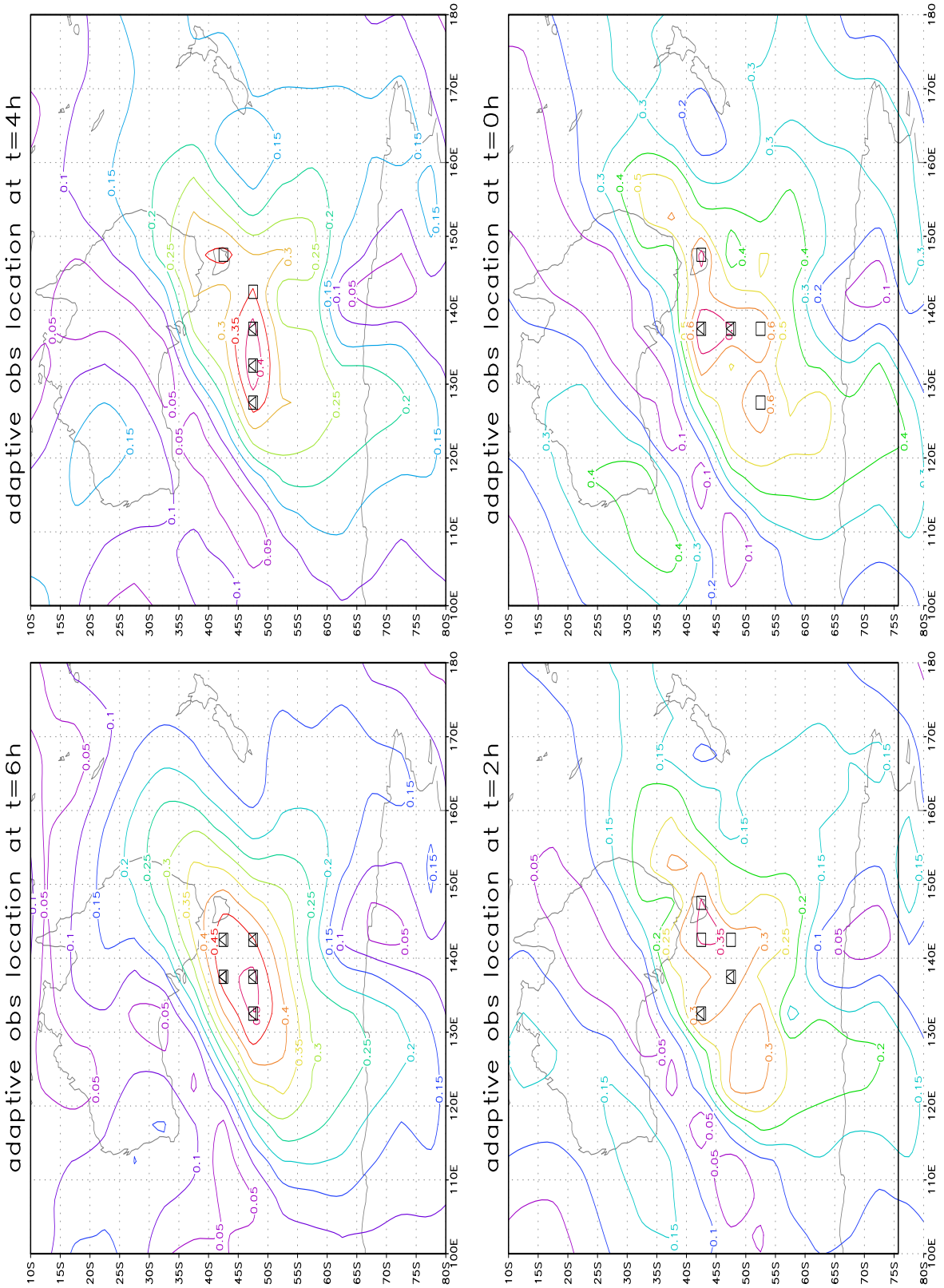
adaptive obs location at t=4h
adaptive obs location at t=6h
adaptive obs location at t=0h
adaptive obs location at t=2h

Figure 8:

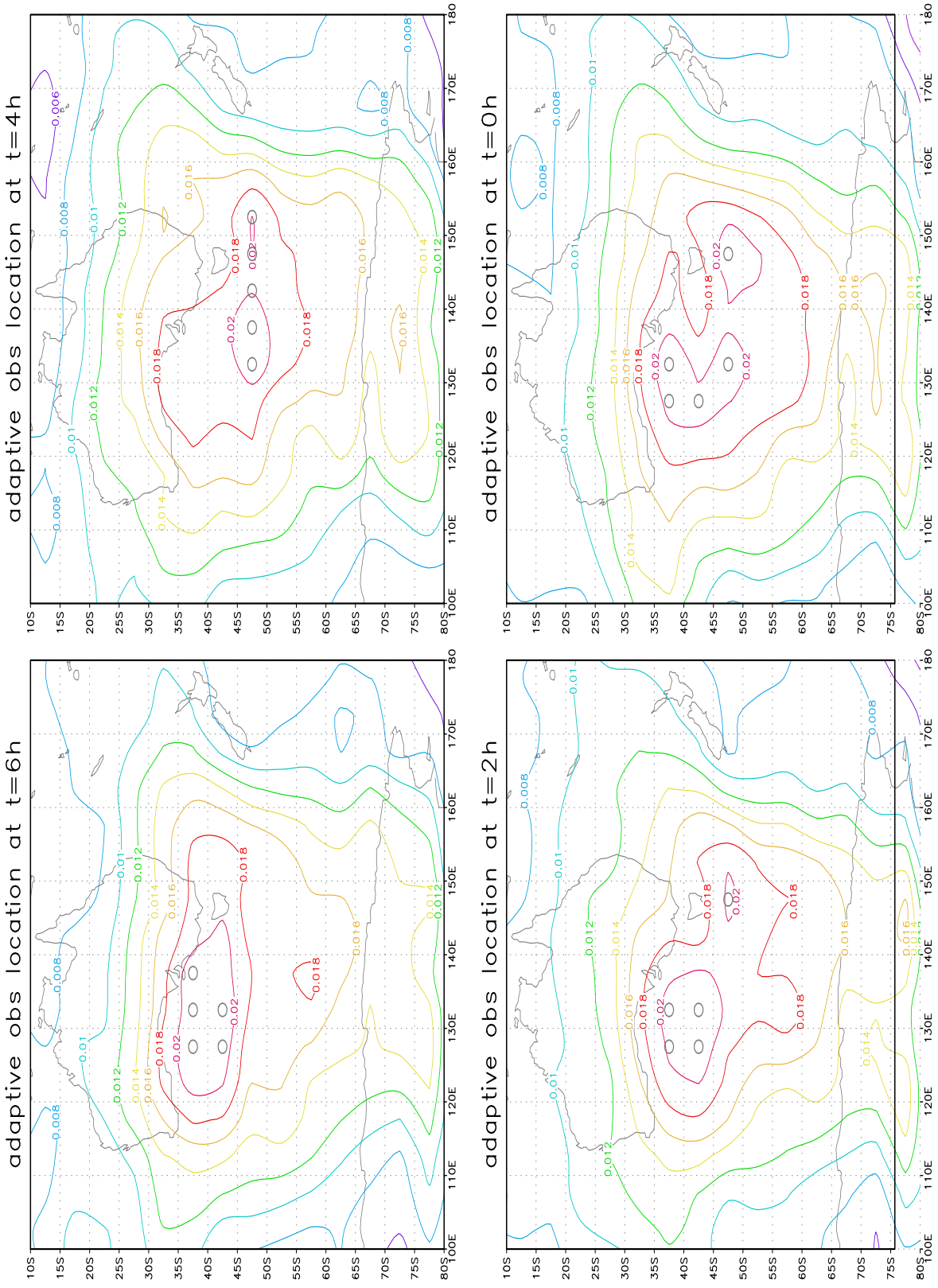
adaptive obs location at t=4h
adaptive obs location at t=0h
adaptive obs location at t=6h
adaptive obs location at t=2h

Figure 9:

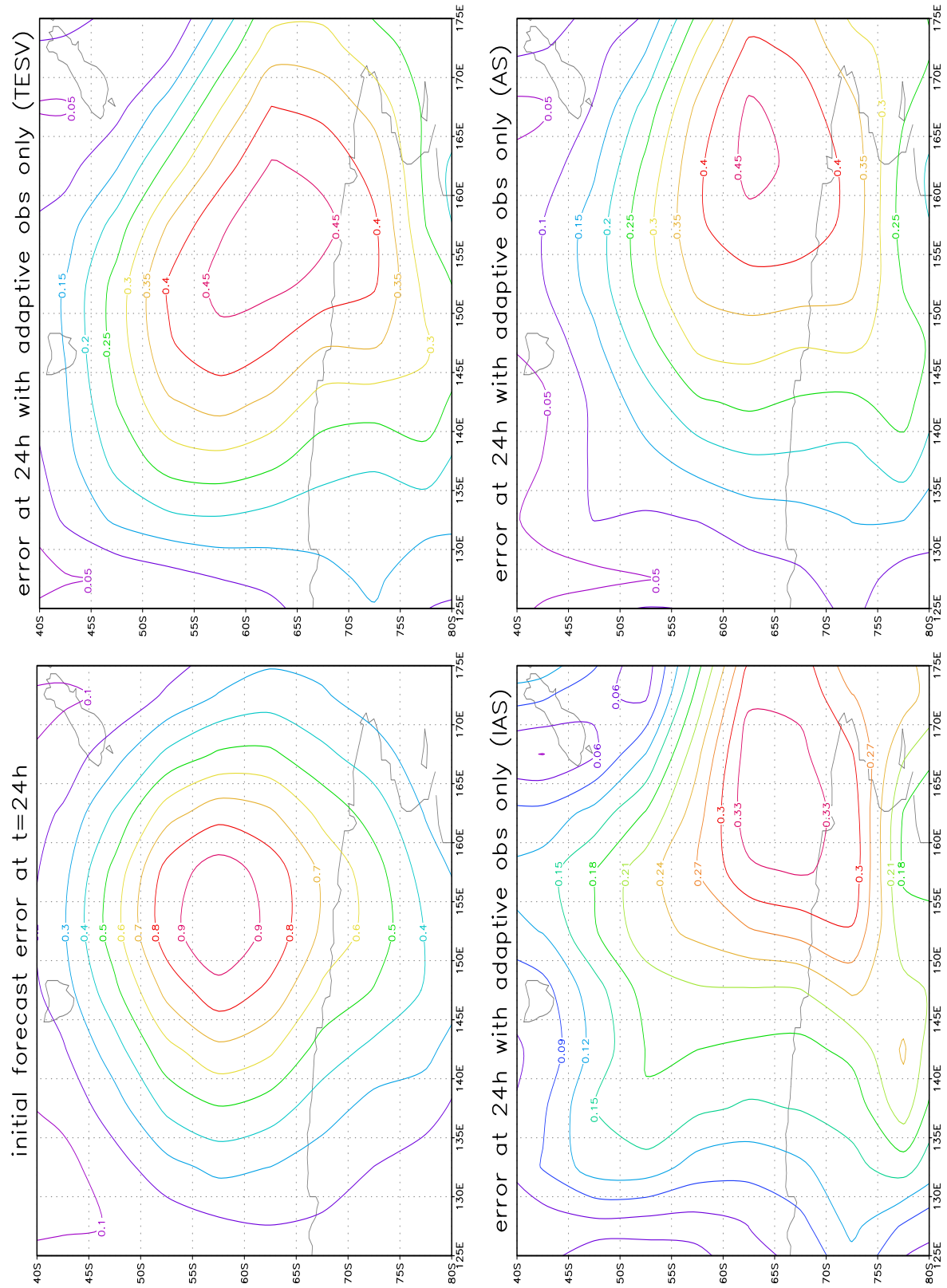
initial forecast error at t=24h
error at 24h with adaptive obs only (TESV)
error at 24h with adaptive obs only (AS)
error at 24h with adaptive obs only (IAS)

Figure 10:

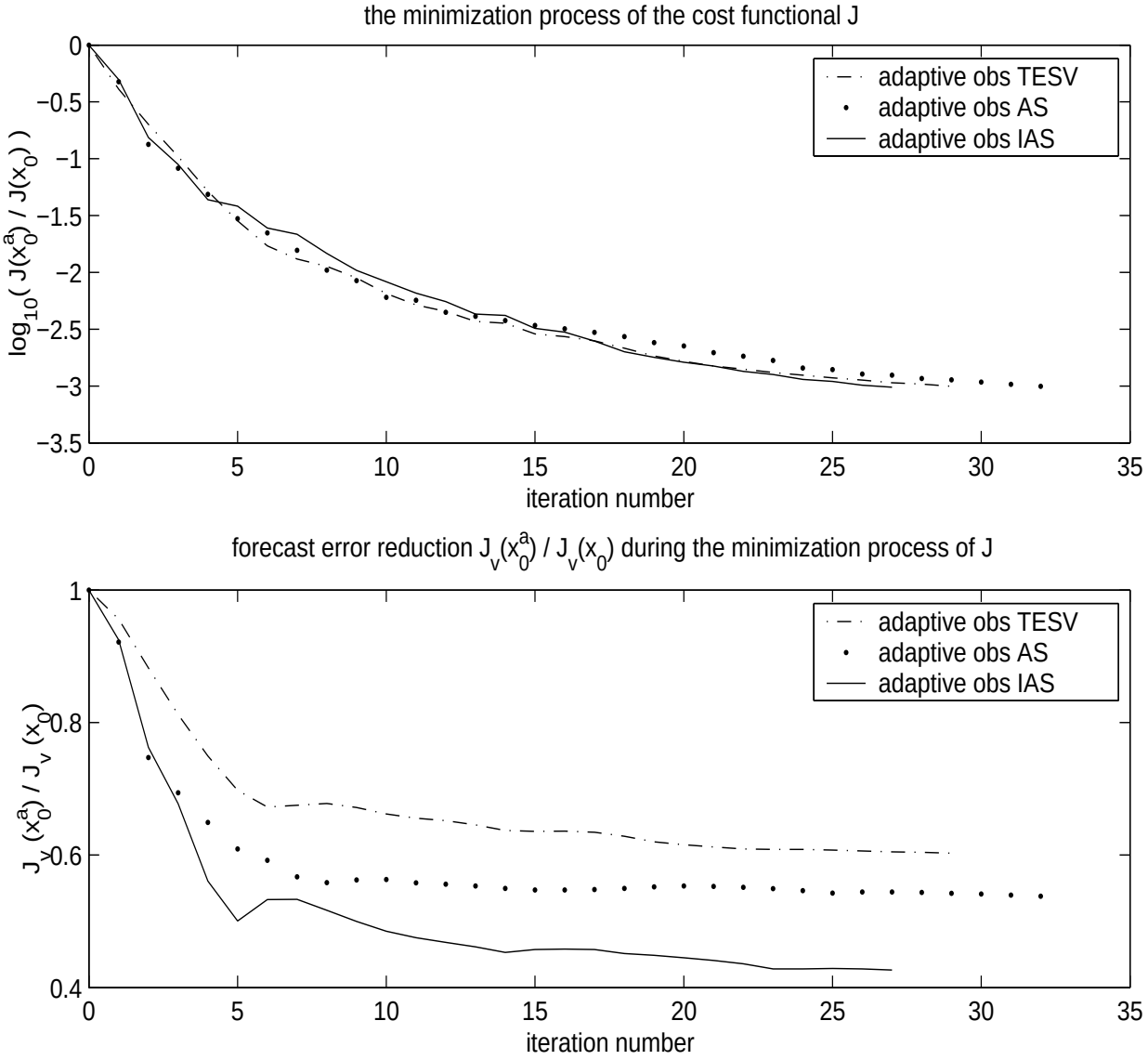
the minimization process of the cost functional J
adaptive obs TESV
adaptive obs AS
adaptive obs IAS
log10(J(x0a) / J(x0))
iteration number
forecast error reduction Jv(x0a) / Jv(x0) during the minimization process of J
adaptive obs TESV
adaptive obs AS
adaptive obs IAS
Jv (x0a) / Jv (x0)
iteration number

Figure 11:

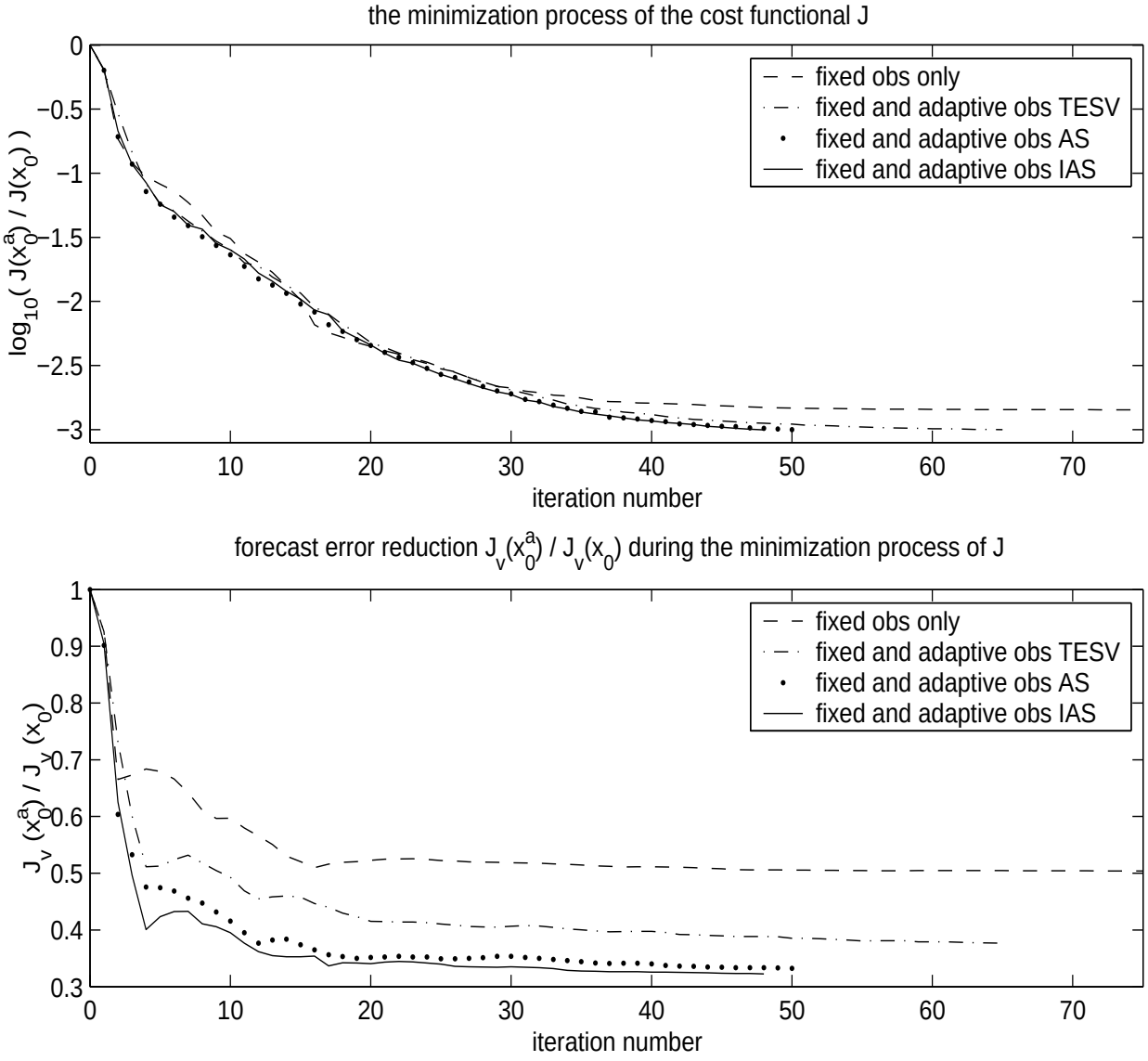
the minimization process of the cost functional J
fixed obs only
fixed and adaptive obs TESV
fixed and adaptive obs AS
fixed and adaptive obs IAS
log10(J(x0a) / J(x0))
iteration number
forecast error reduction Jv(x0a) / Jv(x0) during the minimization process of J
fixed obs only
fixed and adaptive obs TESV
fixed and adaptive obs AS
fixed and adaptive obs IAS
Jv (x0a) / Jv (x0)
iteration number

Figure 12:

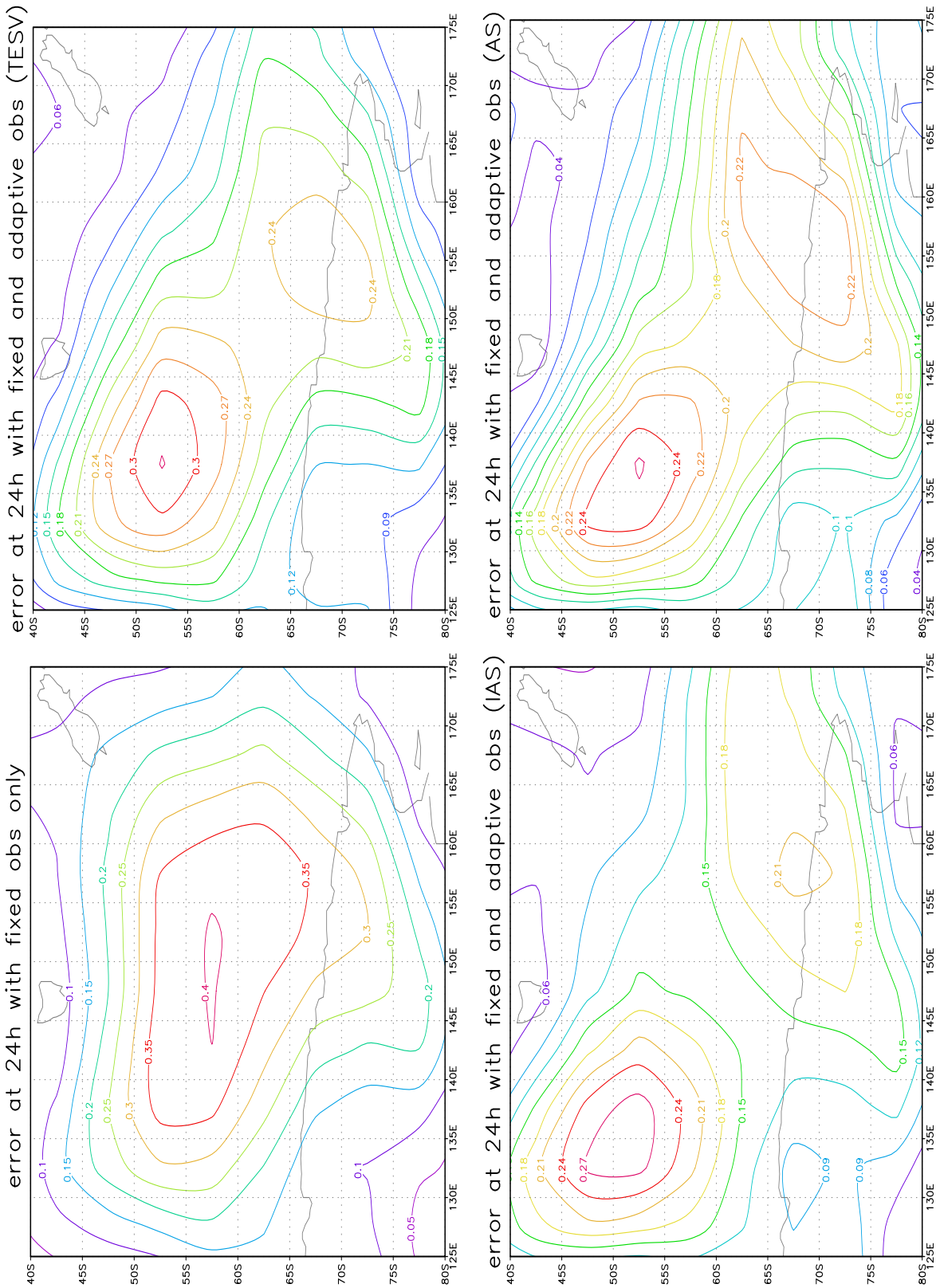
error at 24h with fixed and adaptive obs (TESV)
error at 24h with fixed and adaptive obs (AS)
error at 24h with fixed obs only
error at 24h with fixed and adaptive obs (IAS)

Figure 13:

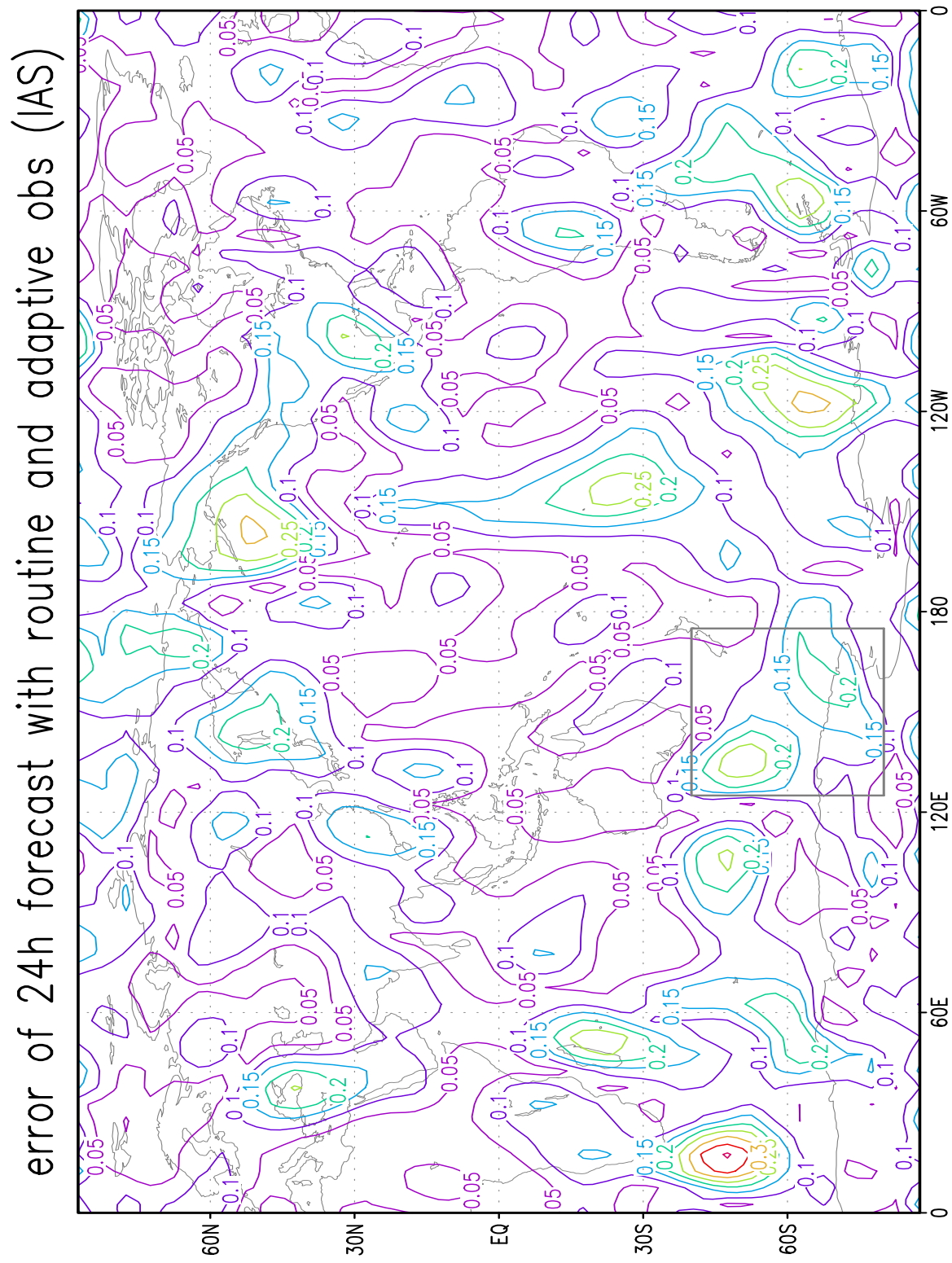
error of 24h forecast with routine and adaptive obs (IAS)
60N
30N
EQ
30S
60S
0
60E
120E
180
120W
60W
0

Figure 14: